Springer

Journal of
Mechanical
Science and
Technology

Journal of Mechanical Science and Technology 23 (2009) 2107~2124

www.springerlink.com/content/1738-494x
DOI 10.1007/s12206-009-0358-8

Geometrically nonlinear vibration analysis of piezoelectrically actuated FGM plate with an initial large deformation †

Farzad Ebrahimi[1, 2,*], Mohammad Hassan Naei[1] and Abbas Rastgoo[1]

[1]*Department of Mechanical Engineering, University of Tehran, Tehran, Iran*
[2]*Mechanical Engineering Department, Faculty of Engineering and Technology, Imam Khomeini International University, Qazvin, Iran*

(Manuscript Received July 15, 2008; Revised Febraury 22, 2009; Accepted March 15, 2009)

Abstract

A theoretical model for geometrically nonlinear vibration analysis of piezoelectrically actuated circular plates made of functionally grade material (FGM) is presented based on Kirchhoff's-Love hypothesis with von-Karman type geometrical large nonlinear deformations. To determine the initial stress state and pre-vibration deformations of the smart plate a nonlinear static problem is solved followed by adding an incremental dynamic state to the pre-vibration state. The derived governing equations of the structure are solved by exact series expansion method combined with perturbation approach. The material properties of the FGM core plate are assumed to be graded in the thickness direction according to the power-law distribution in terms of the volume fractions of the constituents. Control of the FGM plate's nonlinear deflections and natural frequencies using high control voltages is studied and their nonlinear effects are evaluated. Numerical results for FG plates with various mixture of ceramic and metal are presented in dimensionless forms. In a parametric study the emphasis is placed on investigating the effect of varying the applied actuator voltage as well as gradient index of FGM plate on vibration characteristics of the smart structure.

Keywords: Functionally graded material; Geometrically nonlinear vibration; Control; Piezoelectric actuators

1. Introduction

Laminated composite structures can be tailored to design advanced structures, but the sharp change in the properties of each layer at the interface between two adjacent layers causes large inter-laminar shear stresses that may eventually give rise to the well known delamination phenomenon. Such detrimental effects can be mitigated by grading the properties in a continuous manner across the thickness direction, resulting in a new class of materials known as 'functionally graded materials' in which the material properties vary continuously throughout the continuum and specifically in the plates along the thickness direction. For example, Teymur et al. [1] carried out the thermo-mechanical analysis of materials, which are functionally graded in two directions, and demonstrated that the onset of delamination could be prevented by tailoring the microstructures of the composite plies. In an effort to develop the super heat resistant materials, Koizumi [2] first proposed the concept of FGM. These materials which are microscopically heterogeneous and are typically made from isotropic components, such as metals and ceramics, were initially designed as thermal barrier materials for aerospace structures and fusion reactors. But they are now developed for the general use as structural components. Thus, the use of FGM may become an important issue for developing advanced structures. Structures made of FGMs are often susceptible to failure from large deflections, or excessive stresses that are induced by large temperature gradients and/or

† This paper was recommended for publication in revised form by Associate Editor Eung-Soo Shin

*Corresponding author. Tel.: +98 21 8800 5677, Fax.: +98 21 8801 3029
E-mail address: febrahimy@ut.ac.ir

mechanical loads. It is therefore of prime importance to account for the geometrically nonlinear deformation to ensure more accurate and reliable structural analysis and design.

In the quest for developing lightweight high performing flexible structures, a concept emerged to develop structures with self-controlling and self-monitoring capabilities. Expediently, these capabilities of a structure were achieved by exploiting the converse and direct innate effects of the piezoelectric materials as distributed actuators or sensors, which are mounted or embedded in the structure [3, 4]. Such structures having built-in mechanisms for achieving self-controlling and/or self-monitoring capabilities are customarily known as 'smart structures'. The concept of developing smart structures has been extensively used for active control of flexible structures during the past decade [5-7]. In this regard, the use of axisymmetric piezoelectric actuators in the form of a disc or ring to produce motion in a circular or annular substrate plate is common in a wide range of applications including micro-pumps and micro-valves [8, 9], devices for generating and detecting sound [10] and implantable medical devices [11]. They may also be useful in other applications such as microwave microswitches where it is important to control distortion due to intrinsic stresses [12].

To effectively utilize the piezoelectric effect and actuating properties of piezoelectric materials, the interaction between the host structure and piezoelectric patch must be well understood. Compared to the literature on the piezoelectric actuation of beam-like structures, the literature on circular piezoelectric actuators is not extensive. Dobrucki and Pruchnicki [13] developed a finite element method for predicting the dynamic behavior of axisymmetric multilayer shell structures containing piezoelectric layers and with free boundary conditions. They demonstrated the application of the method to a passive circular plate with free edges, carrying a disc actuator on each face. Later, Morris and Forster [14] used the finite element method to optimize a piezoelectric disc actuator with respect to the static deflection of a passive circular plate with fully clamped or ideally pinned boundary conditions. More recently, Dong et al. [9] used the finite element method to predict the deflection of a circular passive plate with pinned boundary condition using a piezoelectric ring actuator. Li and Chen [15] proposed an analytical solution for the deflection of a circular plate, with clamped or pinned boundary conditions, by a piezoelectric disc actuator bonded to the disc. The analysis was based on the assumption of linearly distributed bending strain through the thickness of the different layers. A restricted assumption, that radial and circumferential strains are equal, was also implicitly introduced, thus reducing the two-dimensional model to a one-dimensional model that is quite similar to that of a beam with piezoelectric film actuator [16, 12]. This assumption is valid only for a disc in pure bending loaded with an axisymmetrical moment at the edge [17]. Therefore, the solution is not strictly applicable for an annular actuator.

Most of the studies on piezoelectric systems were based on linear piezoelectricity and linear elasticity theories [18, 19]. Since most structures and elastic continua, especially large lightweight space structures, are flexible, large external static and dynamic excitations can introduce large deformations or geometrical nonlinearity in the structural systems. Accordingly, there is a need to investigate the induced geometrical nonlinear effects on static, dynamic, and control characteristics in order to accurately design and effectively control the structural systems.

Also in recent years, with the increasing use of smart material in vibration control of plate structures, the mechanical response of FGM plates with surface-bonded piezoelectric layers has attracted some researchers' attention. Among those, Ootao and Tanigawa [20] theoretically investigated the simply supported functionally graded (FG) rectangular plate integrated with a piezoelectric plate subjected to transient thermal loading. A 3-D solution for rectangular FG plates coupled with a piezoelectric actuator layer was proposed by Reddy and Cheng [21] using transfer matrix and asymptotic expansion techniques. Wang and Noda [22] analyzed a smart FG composite structure composed of a layer of metal, a layer of piezoelectric and a FG layer in between, while He et al. [23] developed a finite element model for studying the shape and vibration control of FG plates integrated with piezoelectric sensors and actuators. The post buckling behavior of rectangular FG plate with its surface bonded to piezoelectric actuators under the combined action of thermo-electro-mechanical loadings was examined by Liew et al. [24] and Shen [25]; Yang et al. [26] investigated the nonlinear thermo-electro-mechanical bending response of FG rectangular plates that are covered with monolithic piezoelectric actuator layers on the top and bottom surfaces of the plate. They [27] also presented a large amplitude

vibration analysis of a rectangular FG plate with surface-bonded piezoelectric layers by using a semi-analytical method based on 1D differential quadrature and Galerkin technique. Most recently, Huang and Shen [28] investigated the dynamics of an FG plate coupled with two monolithic piezoelectric layers at its top and bottom surfaces undergoing nonlinear vibrations in thermal environments.

All the aforementioned studies focused on the rectangular-shaped plate structures. However, to the authors' best knowledge, no research dealing with the nonlinear vibration characteristics of the circular functionally graded plate integrated with the piezoelectric layers has been reported in literature except the author's recent works in presenting an analytical solution for the free axisymmetric vibration of piezoelectric coupled circular and annular FGM plates [29-33]. In conjunction with these works, in this paper, nonlinear static and dynamic behaviors of a piezoelectric coupled circular functionally graded plate structure with initial large nonlinear deformations (the von-Karman type geometrical nonlinear deformations) are studied. The material properties of the FG core plate are assumed to be graded in the thickness direction according to the power-law distribution in terms of the volume fractions of the constituents while a linear distribution of electric potential field along the thickness of piezoelectric layers is considered. A nonlinear static problem is solved first to determine the initial stress state and pre-vibration deformations of the FG plate that is subjected to in-plane forces and applied actuator voltage in the case of simply supported boundary conditions. By adding an incremental dynamic state to the pre-vibration state, the differential equations that govern the nonlinear vibration behavior of pre-stressed piezoelectric coupled FGM plates are derived. Control effects on nonlinear static deflections and natural frequencies imposed by the piezoelectric actuators using high input voltages are investigated. Numerical examples are provided and simulation results are discussed. Numerical results for FGM plates with a mixture of metal and ceramic are presented in dimensionless forms. The good agreement between the results of this paper and those of the finite element (FE) analyses validated the presented approach. A parametric study is also undertaken to highlight the effects of the applied actuator voltage and material composition of FG core plate on the non vibration characteristics of the composite structure.

2. Functionally graded materials

Nowadays, not only can FGM easily be produced but one can control even the variation of the FG constituents in a specific way. For example, in an FG material made of ceramic and metal mixture, we have

$$V_m + V_c = 1 \tag{1}$$

in which V_c and V_m are the volume fraction of the ceramic and metallic part, respectively. Based on the power law distribution [34], the variation of V_c vs. thickness coordinate (z) with its origin placed at the middle of thickness, can be expressed as:

$$V_c = (z/h_f + 1/2)^n \quad , n \geq 0 \tag{2}$$

in which h_f is the FG core plate thickness, n is the FGM volume fraction index (see Fig. 1). Volume fraction index n dictates the material variation profile across the plate thickness. We assume that the functionally graded plate is made from a mixture of ceramic and metal and the composition varies from the top to the bottom surface; i.e., the top surface of the FGM plate is ceramic-rich (alumina), whereas the bottom surface is metal-rich (aluminum). Typical values for alumina and aluminum are listed in Table 1 [35]. Note that the variation of both constituents (ceramics and metal) is linear when n=1. Moreover, for n=0, a fully ceramic plate is intended. All other mechanical, physical and thermal properties of FGM media follow the same distribution as for V_c. We assume that the inhomogeneous material properties, such as the modulus of elasticity E and the density ρ change within the thickness direction z based on Voigt's rule over the whole range of the volume fraction [36], while Poisson's ratio υ is assumed to be constant in the thickness direction [37] as:

$$\begin{aligned} E(z) &= (E_c - E_m)V_c(z) + E_m \\ \rho(z) &= (\rho_c - \rho_m)V_c(z) + \rho_m \\ \nu(z) &= \nu \end{aligned} \tag{3}$$

where subscripts m and c refer to the metal and ceramic constituents, respectively. After substituting V_c from Eq. (2) into Eqs. (3), material properties of the FGM plate are determined in the power law form which are the same as those proposed by Reddy and Praveen [34] :

Table 1. Material properties [35].

Property	FGM Plate		PZT4
	Alumina	Aluminum	
Young's modulus (GPa)	$E_c = 380$	$E_m = 70$	$E_p = 63$
Density (kg/m^3)	$\rho_c = 3800$	$\rho_m = 2707$	$\rho_p = 7500$
Poisson ratio	0.3	0.3	-
e_{31} (C/m^2)			−4.1

$$E_f(z) = (E_c - E_m)(z/h_f + 1/2)^n + E_m$$
$$\rho_f(z) = (\rho_c - \rho_m)(z/h_f + 1/2)^n + \rho_m \quad (4)$$

3. Nonlinear piezoelectric coupled FG circular plate system

It is assumed that an FGM circular plate is sandwiched between two thin piezoelectric layers which are sensitive in both circumferential and radial directions as shown in Fig. 1 and the piezoelectric layers are much thinner than the FGM plate, i.e., $h_p << h_f$ .An initial large deformation exceeding the linear range is imposed on the circular plate and the von-Karman type nonlinear deformation (nonlinear large deformation or geometrical nonlinearity) is adopted in the analysis. The von-Karman type nonlinearity assumes that the transverse nonlinear deflection w is much more prominent than the other two inplane deflections. In this section, electromechanical system equations of the piezoelectric bounded FG plate are defined, followed by force and moment definitions. The system equations are then simplified to a transverse electromechanical equation when inplane inertia forces and excitations are neglected. Mechanical and electric boundary conditions of the laminated circular plate are also defined.

3.1 Nonlinear strain-displacement relations

The circular FG plate is assumed to be comparatively thin and according to the Kirchhoff's-Love assumptions, normal to the median surface are assumed to remain straight and normal during deformation; thus out-of-plane shear deformations (ε_{zr} , $\varepsilon_{z\theta}$) are disregarded. Strain components at distance z from the middle plane are then given by

$$\varepsilon_{rr} = \bar{\varepsilon}_{rr} + zk_{rr}, \quad \varepsilon_{\theta\theta} = \bar{\varepsilon}_{\theta\theta} + zk_{\theta\theta}, \quad \varepsilon_{r\theta} = \bar{\varepsilon}_{r\theta} + zk_{r\theta} \quad (5)$$

where the z-axis is assumed positive outward. Here $\bar{\varepsilon}_{rr}$, $\bar{\varepsilon}_{\theta\theta}$, $\bar{\varepsilon}_{r\theta}$ are the engineering strain components in the median surface, and k_{rr} , $k_{\theta\theta}$, $k_{r\theta}$ are the curvatures which can be expressed in terms of the displacement components. The relations between the middle plane strains and the displacement components according to the von-Karman type nonlinear deformation (i.e., large deformation or geometrical nonlinearity) and Sander's assumptions are defined as [38]:

$$\bar{\varepsilon}_{rr} = \frac{\partial u_r}{\partial r} + \frac{1}{2}\left(\frac{\partial w}{\partial r}\right)^2$$
$$\bar{\varepsilon}_{\theta\theta} = \frac{1}{r}\frac{\partial u_\theta}{\partial \theta} + \frac{u_r}{r} + \frac{1}{2}\left(\frac{1}{r}\frac{\partial w}{\partial \theta}\right)^2$$
$$\bar{\varepsilon}_{r\theta} = \frac{1}{r}\frac{\partial u_r}{\partial \theta} + \frac{\partial u_\theta}{\partial r} - \frac{u_\theta}{r} + \left(\frac{1}{r}\frac{\partial w}{\partial r}\right)\frac{\partial w}{\partial \theta} \quad (6)$$

$$\kappa_{rr} = -\frac{\partial^2 w}{\partial r^2}$$
$$\kappa_{\theta\theta} = -\frac{1}{r}\frac{\partial w}{\partial r} - \frac{1}{r^2}\frac{\partial^2 w}{\partial \theta^2}$$
$$\kappa_{r\theta} = -\frac{1}{r}\left(\frac{\partial^2 w}{\partial r \partial \theta}\right) + \frac{1}{2r^2}\frac{\partial w}{\partial \theta} \quad (7)$$

where u_r , u_θ ,w represent the corresponding components of the displacement of a point on the middle plate surface. Substituting Eqs. (6) and (7) into Eqs. (5), the following expressions for the strain components are obtained:

$$\varepsilon_{rr} = \frac{\partial u_r}{\partial r} + \frac{1}{2}\left(\frac{\partial w}{\partial r}\right)^2 - z\frac{\partial^2 w}{\partial r^2} \quad (8)$$
$$\varepsilon_{\theta\theta} = \frac{1}{r}\frac{\partial u_\theta}{\partial \theta} + \frac{u_r}{r} + \frac{1}{2}\left(\frac{1}{r}\frac{\partial w}{\partial \theta}\right)^2 - z\left(\frac{1}{r}\frac{\partial w}{\partial r} + \frac{1}{r^2}\frac{\partial^2 w}{\partial \theta^2}\right)$$
$$\varepsilon_{r\theta} = \frac{1}{r}\frac{\partial u_r}{\partial \theta} + \frac{\partial u_\theta}{\partial r} - \frac{u_\theta}{r} + \left(\frac{1}{r}\frac{\partial w}{\partial r}\right)\frac{\partial w}{\partial \theta} + z\left(-\frac{1}{r}\left(\frac{\partial^2 w}{\partial r \partial \theta}\right) + \frac{1}{2r^2}\frac{\partial w}{\partial \theta}\right)$$

Note that the quadratic terms in Eqs. (6)-(8) are nonlinear terms induced by the nonlinear large transverse deflection w.

3.2 Definition of force and moment resultants

The stress components in the FG plate in terms of tensorial strains based on the generalized Hooke's Law are defined as [39]:

$$\sigma_{rr} = \frac{E}{(1-\nu^2)}\left[\varepsilon_{rr} + \nu\varepsilon_{\theta\theta}\right]$$
$$\sigma_{\theta\theta} = \frac{E}{(1-\nu^2)}\left[\varepsilon_{\theta\theta} + \nu\varepsilon_{rr}\right] \quad (9)$$
$$\sigma_{r\theta} = \frac{E}{2(1+\nu)}\varepsilon_{r\theta}$$

The moments and membrane forces include both mechanical and electric components as

$$N_r = N_r^m + N_r^e, \quad N_\theta = N_\theta^m + N_\theta^e,$$
$$N_{r\theta} = N_{r\theta}^m + N_{r\theta}^e, \quad M_r = M_r^m + M_r^e$$
$$M_\theta = M_\theta^m + M_\theta^e, \quad M_{r\theta} = M_{r\theta}^m + M_{r\theta}^e \quad (10)$$

where N^m and N^e are the mechanical and electrical membrane forces and M^m and M^e are the mechanical and electrical bending moments, respectively, and are expressed as

$$(N_r^m, N_\theta^m) = \int_{-h_f/2}^{h_f/2} (\sigma_{rr}, \sigma_{\theta\theta}) dz \quad (11)$$

$$(M_r^m, M_\theta^m) = \int_{-h_f/2}^{h_f/2} (\sigma_{rr}, \sigma_{\theta\theta}) z dz \quad (12)$$

$$(N_{r\theta}^m, M_{r\theta}^m) = \int_{-h_f/2}^{h_f/2} (1, z)\sigma_{r\theta} dz \quad (13)$$

The membrane forces include both mechanical and electric components where the superscript m denotes the mechanical component and e the electric component. The electric components are related to electromechanical couplings or control forces induced by the piezoelectric layers.

Substituting Eqs. (5) and (9) into Eqs. (11)-(13) gives the following constitutive relations for mechanical forces and moments of FG plate in terms of membrane and bending strains which include the nonlinear effects

$$N_r^m = D_1(\bar{\varepsilon}_{rr} + \nu\bar{\varepsilon}_{\theta\theta}), \quad N_\theta^m = D_1(\bar{\varepsilon}_{\theta\theta} + \nu\bar{\varepsilon}_{rr})$$
$$N_{r\theta}^m = \frac{D_1(1-\nu)}{2}\bar{\varepsilon}_{r\theta} \quad (14)$$
$$M_r^m = D_2(\kappa_{rr} + \nu\kappa_{\theta\theta}), \quad M_\theta^m = D_2(\kappa_{\theta\theta} + \nu\kappa_{rr})$$
$$M_{r\theta}^m = \frac{D_2(1-\nu)}{2}\kappa_{r\theta} \quad (15)$$

where the coefficients of D_1 and D_2 in the above equations are related to the plate stiffness and are given by

$$D_1 = \int_{-h_f/2}^{h_f/2} \frac{E_f(z)}{1-\nu_f^2} dz, \; D_2 = \int_{-h_f/2}^{h_f/2} \frac{z^2 E_f(z)}{1-\nu_f^2} dz \quad (16)$$

It is assumed that the piezoelectric layers are sensitive in both radial and circumferential directions and the piezoelectric permeability constants e_{31}=e_{32}. (If there is no mechanical stretch during the manufacturing process, the piezoelectric permeability constants in two inplane directions are equal.) The converse piezoelectric effect is useful in actuators such as ultrasonic welders and ultrasonic motors. Due to this effect a mechanical deformation, i.e., the stress or strain, can be produced when an electric field is applied to the piezoelectric materials in its poled direction. Hence, the electric membrane forces and bending moments are induced by the converse piezoelectric effect on the piezoelectric actuators and these forces vary linearly across the plate thickness as [40]

$$N_r^e = N_\theta^e = e_{31}\left(V_z^t + V_z^b\right)/2, \quad N_{r\theta}^e = 0, \quad (17)$$

$$M_r^e = M_\theta^e = e_{31}\left(h_f + h_p\right)\left(V_z^t - V_z^b\right)/2, \; M_{r\theta}^e = 0, \quad (18)$$

in which V_z^t and V_z^b are the control voltages applied to the top and bottom piezoelectric layers, respectively.

3.3 System electromechanical equations

The system electromechanical equations, in three axial directions, of the piezoelectric coupled circular FG plate (Fig. 1) can be derived from the generic piezoelectric shell equations using four system parameters: two Lame parameters, $A_1 = 1$, $A_2 = a$, and two radii, $R_1 = \infty$, $R_2 = \infty$ [41], and neglecting the in-plane inertia forces we have

$$\frac{\partial(rN_r)}{\partial r} + \frac{\partial N_{r\theta}}{\partial\theta} - N_\theta + q_r^m = 0 \quad (19)$$

$$\frac{\partial(rN_{r\theta})}{\partial r} + \frac{\partial N_\theta}{\partial\theta} + N_{r\theta} + q_\theta^m = 0 \quad (20)$$

$$\frac{1}{r}\frac{\partial(rQ_{rz})}{\partial r} + \frac{1}{r}\frac{\partial Q_{\theta z}}{\partial r} + N_r\frac{\partial^2 w}{\partial r^2} + 2N_{r\theta}\frac{\partial}{\partial r}\left(\frac{1}{r}\frac{\partial w}{\partial\theta}\right) + M_\theta\left[\frac{1}{r}\frac{\partial w}{\partial r} + \frac{1}{r^2}\frac{\partial^2 w}{\partial\theta^2}\right] - I_1\frac{\partial^2 w}{\partial t^2} + q_z^m = 0 \quad (21)$$

where N_{ij} is the membrane force (including both elastic and electric effects) on the ith surface in the jth direction; M_{ij} is the bending moment (also including both elastic and electric effects); q_i^m is the mechanical excitation in the ith direction. When i=j the forces and moments are normal components; i≠j the forces are shear forces and the moments are twists or torques; I_1 and the transverse shear components Q_{rz} and $Q_{\theta z}$ are given as

$$Q_{rz}=\frac{1}{r}\left[\frac{\partial(rM_r)}{\partial r}-M_\theta+\frac{\partial M_{r\theta}}{\partial\theta}\right],$$

$$Q_{\theta z}=\frac{1}{r}\left[\frac{\partial(rM_{r\theta})}{\partial r}-M_{r\theta}+\frac{\partial M_\theta}{\partial\theta}\right],$$

$$I_1=\left(\int_{-h_f/2}^{h_f/2}\rho_f(z)dz\right) \quad (22a,b,c)$$

Excluding inertia forces and external forces, all other force and moment terms are contributed by the FG plate's elasticity and the layers' piezoelectricity.

3.4 Reduced system equation and boundary conditions

To effectively and quantitatively evaluate the nonlinear effect of the piezoelectric bounded FG plate, three governing Eqs. (19)-(21) are simplified to a

Table 2. Values of the normalized dimensionless center deflections with respect to the normalized dimensionless piezoelectric voltages computed by two methods (present series solution and FEM) (ν=0.3, n=10000).

Normalized Voltage (V)	Normalized dimensionless center deflections			Normalized Voltage (V)	Normalized dimensionless center deflections		
	Present	FEM	Diff. (%)		Present	FEM	Diff. (%)
0	0	0	0	1.6	0.8925	0.8930	0.057
0.4	0.3537	0.3538	0.041	2	0.9924	0.9930	0.065
0.8	0.5982	0.5985	0.048	2.4	1.0777	1.0784	0.068
1.2	0.7678	0.7685	0.055	2.8	1.1509	1.1517	0.071
1.4	0.8343	0.8348	0.055	3	1.1827	1.1836	0.073

Table 3. Effect of control voltages to the first natural frequency for various FGM indexes.

Normalized voltage	FGM index (n)						
	Metal	100	10	5	1	0.1	Ceramic
0	*4.8891*	*4.9722*	*5.5359*	*5.9444*	*7.4121*	*10.1803*	*11.2882*
1	*7.2704*	*7.3939*	*8.2323*	*8.8397*	*11.0222*	*15.1388*	*16.7863*
2	*9.3329*	*9.4915*	*10.5677*	*11.3474*	*14.1491*	*19.4335*	*21.5483*
3	*10.7796*	*10.9628*	*12.2058*	*13.1064*	*16.3423*	*22.4459*	*24.8886*
4	*12.0047*	*12.2087*	*13.5929*	*14.5959*	*18.1996*	*24.9968*	*27.7172*

Table 4. Effect of control voltages to the second natural frequency for various FGM indexes.

Normalized voltage	FGM index (n)						
	Metal	100	10	5	1	0.1	Ceramic
0	*29.7205*	*30.2519*	*33.6365*	*35.9718*	*44.7086*	*61.9063*	*68.6434*
1	*30.7844*	*31.3348*	*34.8406*	*37.2595*	*46.3090*	*64.1224*	*71.1006*
2	*32.0353*	*32.6081*	*36.2563*	*38.7735*	*48.1908*	*66.7279*	*73.9897*
3	*33.1552*	*33.7480*	*37.5238*	*40.1290*	*49.8754*	*69.0606*	*76.5763*
4	*34.0349*	*34.6434*	*38.5194*	*41.1937*	*51.1988*	*70.8930*	*78.6081*

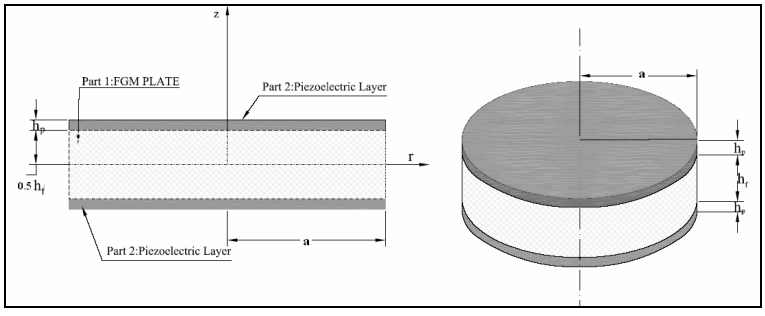

Fig. 1. Schematic representation of the FG circular plate coupled with two piezoelectric layers.

manageable form based on their physical significances. For a uniformly distributed piezoelectric layer, electric potentials (V_z^t and V_z^b) are independent of the spatial coordinates r and θ. Thus, Eqs. (19) and (20) can be satisfied by using an Airy's stress function $\phi(r,\theta)$ [42] by redefining the forces as

$$N_r^m = \left(\frac{1}{r}\frac{\partial\phi}{\partial r} + \frac{1}{r^2}\frac{\partial^2\phi}{\partial\theta^2}\right), \quad N_\theta^m = \frac{\partial^2\phi}{\partial r^2},$$
$$N_{r\theta}^m = -\frac{\partial}{\partial r}\left(\frac{1}{r}\frac{\partial\phi}{\partial\theta}\right). \tag{23}$$

Then, using the transverse electromechanical Eq. (21), the bending strain Eqs. (7) and the moment definitions (14), one can redefine the transverse electromechanical equation of the circular FG plate as

$$D_2\Delta\Delta w(r,\theta) = q_z^m(r,\theta) - I_1\frac{\partial^2 w}{\partial t^2} + h_f \times$$
$$\left[\frac{\partial^2\phi}{\partial r^2}\left(\frac{1}{r}\frac{\partial w}{\partial r} + \frac{1}{r^2}\frac{\partial^2 w}{\partial\theta^2}\right) + \left(\frac{1}{r}\frac{\partial\phi}{\partial r} + \frac{1}{r^2}\frac{\partial^2\phi}{\partial\theta^2}\right)\frac{\partial^2 w}{\partial r^2}\right.$$
$$\left. -2\frac{\partial}{\partial r}\left(\frac{1}{r}\frac{\partial\phi}{\partial\theta}\right)\frac{\partial}{\partial r}\left(\frac{1}{r}\frac{\partial w}{\partial\theta}\right)\right] - N_r^e \tag{24}$$

in which N_r^e is independent of r and θ coordinates as given in Eq. (17) and Δ is the Laplacian operator in cylindrical coordinate system and is given by

$$\Delta = \frac{\partial^2}{\partial r^2} + \frac{\partial}{r\partial r} + \frac{\partial^2}{r^2\partial\theta^2} \tag{25}$$

Eliminating the displacements u_r and u_θ from the inplane displacement-strain Eqs. (6), then substituting the stress functions (14) and (23) into the combined equation with the transverse coordinate w, one can derive a compatible equation as

$$\Delta\Delta\phi(r,\theta) = \left(\int_{-h_f/2}^{h_f/2} E_f(z)dz\right)\times$$
$$\left[\left[\frac{\partial}{\partial r}\left(\frac{1}{r}\frac{\partial w}{\partial\theta}\right)\right]^2 - \frac{\partial^2 w}{\partial r^2}\left(\frac{1}{r}\frac{\partial w}{\partial r} + \frac{1}{r^2}\frac{\partial^2 w}{\partial\theta^2}\right)\right] \tag{26}$$

For a circular plate simply supported on its circumference, the boundary conditions on the circumference ($r=a$) are defined as

$$w = 0, \quad u_r = 0, \quad M_r^m = M_r^e \tag{27}$$

It is further assumed that only axisymmetric plate deformations are considered; thus, the nonlinear transverse electromechanical Eqs. (24) and (26) can be reduced to the following transverse axisymmetric oscillation equations:

$$\frac{D_2}{r}\frac{\partial}{\partial r}\left(r\frac{\partial}{\partial r}\left[\frac{1}{r}\frac{\partial}{\partial r}\left(r\frac{\partial}{\partial r}w\right)\right]\right) =$$
$$q_z^m(r) + \frac{1}{r}\frac{\partial}{\partial r}\left(rN_r^m\frac{\partial w}{\partial r}\right) - N_r^e\frac{1}{r}\frac{\partial}{\partial r}\left(r\frac{\partial w}{\partial r}\right) - I_1\frac{\partial^2 w}{\partial t^2} \tag{28}$$

$$r\frac{\partial}{\partial r}\left(\frac{1}{r}\frac{\partial}{\partial r}\left(r^2N_r^m\right)\right) = -\frac{1}{2}\left(\int_{-h_f/2}^{h_f/2} E_f(z)dz\right)\left(\frac{\partial w}{\partial r}\right)^2 \tag{29}$$

Boundary conditions for axisymmetric oscillations are defined as:

Plate center ($r=0$):

$$\frac{\partial w}{\partial r} = 0 \quad N_r^m : \text{finite} \tag{30}$$

Plate circumference ($r=a$):

$$w = 0 \quad -D_2\left(\frac{\partial^2 w}{\partial r^2} + \frac{\nu}{r}\frac{\partial w}{\partial r}\right) = M_r^e$$
$$\frac{\partial}{\partial r}(rN_r^m) - \nu N_r^m = 0 \tag{31}$$

Note that Eqs. (28)-(31) constitute the governing nonlinear electromechanical equations and boundary conditions for the nonlinear piezoelectric embedded FG circular plate with nonlinear axisymmetric deformation and vibration. Since vibration analysis is referenced to the nonlinearly deformed static equilibrium position, a nonlinear static problem is solved first to determine the initial stress state and pre-vibration deformations of the plate that is subjected to applied actuator voltage. By adding an incremental dynamic state to the pre-vibration state, the differential equations that govern the nonlinear vibration behavior of pre-stressed structure with initial nonlinear deformations are derived. Then the control effects induced by the piezoelectric actuators are evaluated.

4. Nonlinear pre-vibration analysis

In this section, voltage-induced static deformations of the circular FG plate with large deformations are studied. It is assumed that the external mechanical excitation is zero and control voltages applied to the top and bottom piezoelectric layers are of equal magnitude and opposite signs such that an electric bound-

ary control moment is generated on the plate circumference as

$$V_z^t = -V_z^b = V^* \tag{32}$$

In addition, the inplane electric force vanishes due to Eq. (32). Simplifying the dynamic electromechanical Eqs. (28) and (29) yields the nonlinear static equations as

$$\frac{D_2}{r}\frac{d}{dr}\left(r\frac{d}{dr}\left[\frac{1}{r}\frac{d}{dr}\left(r\frac{d}{dr}w_s\right)\right]\right) = \frac{1}{r}\frac{d}{dr}\left(rN_{r_s}^m\frac{dw_s}{dr}\right) \tag{33a}$$

$$r\frac{d}{dr}\left(\frac{1}{r}\frac{d}{dr}(r^2N_{r_s}^m)\right) = -\frac{1}{2}\left(\int_{-h_f/2}^{h_f/2}E_f(z)dz\right)\left(\frac{dw_s}{dr}\right)^2 \quad 0\langle r\langle a \tag{33b}$$

The boundary conditions at the plate center and circumference are redefined for the static equilibrium position as

(1) *r=0*:

$$\frac{dw_s}{dr} = 0\,,\quad N_{r_s}^m : \text{finite} \tag{34a,b}$$

(2) *r=a:*

$$w_s = 0\,,\quad \frac{\partial}{\partial r}(rN_{r_s}^m) - \nu N_{r_s}^m = 0\,,$$

$$-D_2\left(\frac{d^2w_s}{dr^2} + \frac{\nu}{r}\frac{dw_s}{dr}\right) = M_{r_s}^e \tag{35a,b,c}$$

where the electric moment is defined as

$$M_{r_s}^e = e_{31}\left(h_f + h_p\right)V^* \tag{36}$$

To facilitate the analysis, normalized dimensionless quantities are adopted in static and dynamic analyses as follows [43]:

$$y = \left(\frac{r}{a}\right)^2,\quad W_s = \sqrt{3\left(1-\nu^2\right)}\frac{w_s}{h_f}\,,$$

$$X_s(y) = y\frac{dW_s}{dy},\quad Y_s^m(y) = \left[\frac{a^2N_{r_s}^m}{4D_2}\right]y$$

$$P_s^m(y) = \sqrt{3(1-\nu^2)}\left(\frac{M_{r_s}^m a^2}{2D_2h_f}\right),$$

$$P_s^e(y) = \sqrt{3(1-\nu^2)}\left(\frac{M_{r_s}^e a^2}{2D_2h_f}\right) \tag{37}$$

The nonlinear static equations and boundary conditions (33)-(35) can be normalized in a dimensionless form. The dimensionless static equations and boundary conditions become

$$y^2\frac{d^2X_s(y)}{dy^2} = X_s(y)Y_s^m(y)\,, \tag{38a}$$

$$y^2\frac{d^2Y_s^m(y)}{dy^2} = -\frac{1}{2}\left(X_s(2y)\right)^2,\quad 0 < y < 1 \tag{38b}$$

$$X_s(0) = 0\,,\quad Y_s^m(0) = 0\quad (y = 0) \tag{39a,b}$$

$$\left(1+\nu\right)Y_s^m(1) - 2\frac{dY_s^m(1)}{dy} = 0\,,$$

$$\left(1-\nu\right)X_s(1) - 2\frac{dX_s^m(1)}{dy} = -P_s^e\quad (y = 1) \tag{40a,b}$$

For the nonlinear static equations and boundary conditions derived above, static solutions $X_s(y)$ and $Y_s^m(y)$ can be assumed in exact series expansion forms [43] as

$$X_s(y) = \sum_{i=1}^{\infty}A_iy^i \quad Y_s^m(y) = \sum_{i=1}^{\infty}B_iy^i \tag{41a,b}$$

where A_i and B_i are coefficients. Solving the coupled static equations gives the dimensionless slope $X_s(y)$, and integrating the slope gives the dimensionless static deflection $W_s(y)$ as:

$$W_s(y) = -\int_y^1\frac{1}{\xi}X_s(\xi)d\xi\,, \tag{42}$$

Substituting the series solutions (41a, b) into the system equations and boundary conditions (38)-(40), one can derive recurrence equations for the solution coefficients A_i and B_i as:

$$A_i = \frac{1}{i\left(i-1\right)}\sum_{j=1}^{i-1}A_jB_{i-j}\,,$$

$$B_i = \frac{-1}{2i\left(i-1\right)}\sum_{j=1}^{i-1}A_jA_{i-j}\,,\quad i = 2,3,4,... \tag{43a,b}$$

and boundary conditions

$$\sum_{i=1}^{\infty}\left[\left(1+\nu-2i\right)B_i\right] = 0\,,$$

$$\sum_{i=1}^{\infty}\left[\left(1-\nu-2i\right)A_i\right]+P_s^e=0 \qquad (44a,b)$$

The recurrence Eqs. (43a, b) suggest that only A_1 and B_1 are independent coefficients determined by the nonlinear algebraic boundary Eqs. (44a, b). Using the Newton-Raphson method [44], one can solve the nonlinear boundary equations and determine the normalized plate displacement in an exact series expansion form. Accordingly, nonlinear (static) control effects can be investigated.

5. Nonlinear vibration analysis and amplitude-frequency relations

5.1 Nonlinear vibration analysis

The free vibration analysis with piezoelectric control effects is assumed in the vicinity of nonlinearly deformed static equilibrium position. Frequency control or variation of the circular plate with an initial nonlinear deformation is studied in this section. We assume that the solutions of the nonlinear dynamic Eqs. (28)-(31) include a static component and a dynamic component as:

$$w(r,t)=w_s(r)+w_d(r,t)\ ,$$
$$N_r^m(r,t)=N_{r_s}^m(r,t)+N_{r_d}^m(r,t) \qquad (45a,b)$$

Substituting the assumed solutions (45a, b) into the original dynamic equations and boundary conditions (28)-(31) and subtracting corresponding terms in the nonlinear static equations and boundary conditions (33)-(35), one can derive the nonlinear dynamic equations in the vicinity of nonlinear deformed geometry as:

$$\frac{D_2}{r}\frac{\partial}{\partial r}\left(r\frac{\partial}{\partial r}\left[\frac{1}{r}\frac{\partial}{\partial r}\left(r\frac{\partial}{\partial r}w_d\right)\right]\right)=-I_1\frac{\partial^2 w_d}{\partial t^2}+\frac{1}{r}\frac{\partial}{\partial r}\left[rN_{r_d}^m\frac{dw_s}{dr}+rN_{r_s}^m\frac{\partial w_d}{\partial r}+rN_{r_d}^m\frac{\partial w_d}{\partial r}\right] \qquad (46a)$$

$$r\frac{\partial}{\partial r}\left[\frac{1}{r}\frac{\partial}{\partial r}(r^2N_{r_d}^m)\right]=-\frac{1}{2}\left(\int_{-h_f/2}^{h_f/2}E_f(z)dz\right)\left[2\frac{dw_s}{dr}\frac{\partial w_d}{\partial r}+\left(\frac{\partial w_d}{\partial r}\right)^2\right],\ 0<r<a \qquad (46b)$$

The boundary conditions are defined as

(1) $r=0$:

$$\frac{\partial w_d}{\partial r}=0\ ,\quad N_{r_d}^m:\text{finite;} \qquad (47a,b)$$

(2) $r=a$:

$$w_d=0\ ,\quad \frac{\partial}{\partial r}(rN_{r_d}^m)-\nu N_{r_d}^m=0\ ,\quad -D_2\left(\frac{\partial^2 w_d}{\partial r^2}+\frac{\nu}{r}\frac{\partial w_d}{\partial r}\right)=0 \qquad (48a,b,c)$$

Again, we define the normalized dimensionless quantities as:

$$x=\frac{r}{a}\ ,\quad \bar{w}_d=2\sqrt{3\left(1-\nu^2\right)}\frac{w_d}{h_f}\ ,$$
$$\bar{N}_{r_d}^m=\frac{a^2N_{r_d}^m}{D_2}\ ,\ \bar{w}_s=2\sqrt{3\left(1-\nu^2\right)}\frac{w_s}{h_f}$$
$$\bar{N}_{r_s}^m=\frac{a^2N_{r_s}^m}{D_2}\ ,\quad \lambda=I_1\frac{a^4}{D_2}\omega_n^2\ ,\quad \tau=\omega_n t \qquad (49)$$

The nonlinear dynamic equations can be normalized in a dimensionless form:

$$\frac{1}{x}\frac{\partial}{\partial x}\left\{x\frac{\partial}{\partial x}\left[\frac{1}{x}\frac{\partial}{\partial x}\left(x\frac{\partial}{\partial x}(\bar{w}_d)\right)\right]\right\}=-\lambda\frac{\partial^2\bar{w}_d}{\partial\tau^2}+\frac{1}{x}\frac{\partial}{\partial x}\left[x\bar{N}_{r_d}^m\frac{d\bar{w}_s}{dx}+x\bar{N}_{r_s}^m\frac{\partial\bar{w}_d}{\partial x}+x\bar{N}_{r_d}^m\frac{\partial\bar{w}_d}{\partial x}\right] \qquad (50a)$$

$$x\frac{\partial}{\partial x}\left(\frac{1}{x}\frac{\partial}{\partial x}\left[x^2\bar{N}_{r_d}^m(x,\tau)\right]\right)=-\left[\frac{d\bar{w}_s}{dx}\frac{\partial\bar{w}_d}{\partial x}+\frac{1}{2}\left(\frac{\partial\bar{w}_d}{\partial x}\right)^2\right],\ 0<x<1 \qquad (50b)$$

The normalized dimensionless boundary conditions become

$$\frac{\partial\bar{w}_d}{\partial x}=0\ ,\quad \bar{N}_{r_d}^m:\text{finite, at (x=0)} \qquad (51a,b)$$

$$\bar{w}_d=0\ ,\quad \frac{\partial}{\partial x}(x\bar{N}_{r_d}^m)-\nu\bar{N}_{r_d}^m=0\ ,\quad \frac{\partial^2\bar{w}_d}{\partial x^2}+\frac{\nu}{x}\frac{\partial\bar{w}_d}{\partial x}=0\ ,\text{ at (x=1)} \qquad (52a,b,c)$$

Eqs. (50)-(52) constitute the dimensionless nonlinear dynamic equations (in axisymmetric transverse oscillation) and boundary conditions of the piezoelectric laminated FG circular plate with initial nonlinear deformations. Solutions for the linear eigenvalue problems are derived first and then extended to in-

clude nonlinear perturbation effects.

5.2 Solutions for eigenvalue problem

Assuming harmonic solutions for $\bar{w}_d(x,\tau)$ and $\bar{N}^m_{r_d}(x,\tau)$ in the free vibration analysis as:

$$\bar{w}_d(x,\tau)=R_d(x)\sin\tau\ ,\quad \bar{N}^m_{r_d}(x,\tau)=S_d(x)\sin\tau\ , \tag{53a,b}$$

in which $R_d(x)$ defines the mode shape function and $S_d(x)$ defines the spatial force distribution. Substituting Eqs. (53) into Eq. (50) gives the eigenvalue equations as

$$\frac{1}{x}\frac{d}{dx}\left\{x\frac{d}{dx}\left[\frac{1}{x}\frac{d}{dx}\left(x\frac{d}{dx}(R_d(x))\right)\right]\right\}=$$
$$\lambda R_d(x)+\frac{1}{x}\frac{d}{dx}\left[xS_d(x)\frac{d\bar{w}_s}{dx}+x\bar{N}^m_{r_s}\frac{dR_d}{dx}\right]$$
$$x\frac{d}{dx}\left(\frac{1}{x}\frac{d}{dx}\left[x^2S_d(x)\right]\right)=-\frac{d\bar{w}_s}{dx}\frac{dR_d}{dx}\ , \tag{54a,b}$$

The boundary conditions become

$$\frac{dR_d}{dx}=0\ ,\quad S_d(x)\text{ : finite at (x=0)} \tag{55}$$

$$R_d=0\ ,\quad \frac{d}{dx}(xS_d(x))-\nu S_d(x)=0\ ,$$
$$\frac{d^2R_d}{dx^2}+\frac{\nu}{x}\frac{dR_d}{dx}=0\quad\text{at } (x=1) \tag{56}$$

Using the first four dimensionless terms in Eqs. (37) , the series solutions (41a, b) and the third and fifth terms in Eq. (49), one can derive the static solutions $d\bar{w}_s/dx$ and $\bar{N}^m_{r_s}$ as

$$\frac{d\bar{w}_s}{dx}=\sum_{i=1}^{\infty}\bar{A}_ix^{2i-1}\ ,\quad \bar{N}^m_{r_s}=\sum_{i=1}^{\infty}\bar{B}_ix^{2i} \tag{57a,b}$$

in which the coefficients are

$$\bar{A}_i=4A_i\ ,\quad \bar{B}_{i-1}=4B_i\ ,\quad i=1,2,3,... \tag{58a,b}$$

Using the static solutions (57a, b), one can write the series-type eigenfunctions $R_d(x)$ and $S_d(x)$ in the form

$$R_d(x)=\sum_{i=0}^{\infty}a_ix^{2i}\ ,\quad S_d(x)=\sum_{i=0}^{\infty}b_ix^{2i} \tag{59a,b}$$

in which a_i and b_i are constants determined by the eigenvalue equations and boundary conditions (54)-(56). Substituting static solutions (57a, b) and series eigenfunctions (59a, b) into the eigenvalue equations and boundary conditions (54)-(56) and solving for constants a_i and b_i gives

$$b_i=-\frac{1}{2i(i+1)}\sum_{j=1}^{i}ja_j\bar{A}_{i-j+1}\ ,\quad i=1,2,3,... \tag{60a}$$

$$a_2=\frac{1}{64}\left[\lambda a_0+2\left(2a_1\bar{B}_0+\bar{A}_1b_0\right)\right], \tag{60b}$$

$$a_3=\frac{1}{576}\left[\lambda a_1+4\left(2a_1\bar{B}_1+\bar{A}_1b_1+4a_2\bar{B}_0+\bar{A}_2b_0\right)\right] \tag{60c}$$

$$a_{i+2}=\frac{1}{16(i+1)^2(i+2)^2}\times$$
$$\left[\lambda a_i+2(i+1)\sum_{j=1}^{i+1}\left(2ja_j\bar{B}_{i-j+1}+\bar{A}_jb_{i-j+1}\right)\right]\quad i=2,3,4,... \tag{60d}$$

$$\sum_{i=0}^{\infty}a_i=0\ ,\quad \sum_{i=0}^{\infty}(2i-1+\nu)ia_i=0\ ,$$
$$\sum_{i=0}^{\infty}(2i+1-\nu)b_i=0 \tag{61a,b,c}$$

Note that only a_0 , a_1 and b_0 are independent constants for the eigenfunctions $R_d(x)$ and $S_d(x)$. The next step is to search for their nonzero solutions, i.e., solutions of $R_d(x)\neq 0$, which correspond to a_0 , a_1 and b_0 not simultaneously being zero for an eigenvalue λ . Using the condition of nonzero solutions of the homogeneous algebraic equations, one can determine the eigenvalue λ and consequently the corresponding eigenfunction.

5.3 Amplitude-frequency relations for large amplitude vibrations

It is known that the frequency changes with respect to the vibration amplitude in nonlinear oscillations. In this section, the perturbation method is used to investigate the nonlinear deformation (large amplitude) effect at natural frequencies of the piezoelectric bounded FGM circular plate. One can define an integral equation for the radial membrane force $\bar{N}^m_{r_d}(x,\tau)$ [43],

$$\bar{N}^m_{r_d}(x,\tau)=$$
$$\frac{1}{2x^2}\int_0^1 G(x,\xi)\frac{1}{\xi}\left[\frac{d\bar{w}_s}{d\xi}\frac{\partial\bar{w}_d}{\partial\xi}+\frac{1}{2}\left(\frac{\partial\bar{w}_d}{\partial\xi}\right)^2\right]d\xi=\bar{N}^{*1}_{r_d}(x)+\bar{N}^{*n}_{r_d}(x) \tag{62}$$

in Eq. (50b) and boundary conditions (51b) and (52b). $\bar{N}^{*l}_{r_d}(x)$ and $\bar{N}^{*n}_{r_d}(x)$ are the linear component and nonlinear components, respectively. $G(x,\xi)$ is a kernel function and is defined as:

$$G(x,\xi)=\begin{cases}\left[\left((1-\nu)/(1+\nu)\right)\xi^2+1\right]x^2 & x<\xi,\\ \left[\left((1-\nu)/(1+\nu)\right)x^2+1\right]\xi^2 & x>\xi,\end{cases} \tag{63}$$

The nonlinear dynamic equation of large amplitude free vibration in the vicinity of the nonlinearly deformed static equilibrium position can be written as

$$\begin{aligned}&\frac{1}{x}\frac{\partial}{\partial x}\left\{x\frac{\partial}{\partial x}\left[\frac{1}{x}\frac{\partial}{\partial x}\left(x\frac{\partial}{\partial x}(\bar{w}_d)\right)\right]\right\}=\\ &-\lambda\frac{\partial^2\bar{w}_d}{\partial\tau^2}+\frac{1}{x}\frac{\partial}{\partial x}\left[x\bar{N}^m_{r_d}\frac{d\bar{w}_s}{dx}+x\bar{N}^m_{r_s}\frac{\partial\bar{w}_d}{\partial x}+x\bar{N}^m_{r_d}\frac{\partial\bar{w}_d}{\partial x}\right]\end{aligned} \tag{64}$$

with the boundary conditions

Plate center x=0: $\dfrac{\partial\bar{w}_d}{\partial x}=0$ (65)

(2) Plate circumference x=1:

$$\bar{w}_d=0\,,\quad \frac{\partial^2\bar{w}_d}{\partial x^2}+\frac{\nu}{x}\frac{\partial\bar{w}_d}{\partial x}=0\,, \tag{66a,b}$$

It should be recalled that the boundary membrane force at $x=1$ was defined in Eq. (62). Assume an approximate solution of the nonlinear response $\bar{w}_d(x,\tau)$ to be a product of a spatial function $\bar{w}^*_d(x)$ and a temporal function $f(\tau)$,

$$\bar{w}_d(x,\tau)=\bar{w}^*_d(x)f(\tau)\,, \tag{67}$$

where $\bar{w}^*_d(x)$ is a test function which satisfies boundary conditions of Eqs. (65) and (66) and here is taken as the exact series-type eigenfunction $R_d(x)$ in Eq. (59a). Substituting Eq. (67) into Eq. (64) and imposing the Galerkin method yields an equation of the temporal function $f(\tau)$ as:

$$\begin{aligned}&f_{,\tau\tau}+f+\mu_1f^2+\mu_2f^3=0\,,\quad \mu_1=c_3/c_2\,,\\ &\mu_2=c_4/c_2\end{aligned} \tag{68}$$

where the coefficients c_1 and c_2 are linear parts and c_3 and c_4 are nonlinear parts; the eigenvalue λ is defined as

$$\lambda=c_2/c_1\,, \tag{69}$$

The coefficients c_i are defined by integral equations as:

$$c_1=\int_0^1\left(\bar{w}^*_d(x)\right)^2x\,dx \tag{70a}$$

$$c_2=\int_0^1\left\{\begin{aligned}&\frac{1}{x}\frac{d}{dx}\left\{x\frac{d}{dx}\left[\frac{1}{x}\frac{d}{dx}\left(x\frac{d}{dx}(\bar{w}^*_d(x))\right)\right]\right\}\\ &-\frac{1}{x}\frac{d}{dx}\left[x\bar{N}^m_{r_s}(x)\frac{d\bar{w}^*_d}{dx}+x\bar{N}^{*l}_{r_d}(x)\frac{d\bar{w}_s}{dx}\right]\end{aligned}\right\}\bar{w}^*_d(x)x\,dx \tag{70b}$$

$$c_3=-\int_0^1\frac{1}{x}\frac{d}{dx}\left[x\bar{N}^{*n}_{r_d}(x)\frac{d\bar{w}_s}{dx}+x\bar{N}^{*l}_{r_d}(x)\frac{d\bar{w}^*_d}{dx}\right]\bar{w}^*_d(x)x\,dx \tag{70c}$$

$$c_4=-\int_0^1\frac{1}{x}\frac{d}{dx}\left[x\bar{N}^{*n}_{r_d}(x)\frac{d\bar{w}^*_d(x)}{dx}\right]\bar{w}^*_d(x)x\,dx \tag{70d}$$

in which

$$\bar{N}^{*l}_{r_d}(x)=\frac{1}{2x^2}\int_0^1G(x,\xi)\frac{1}{\xi}\frac{d\bar{w}_s}{d\xi}\frac{d\bar{w}^*_d}{d\xi}d\xi \tag{71a}$$

$$\bar{N}^{*n}_{r_d}(x)=\frac{1}{4x^2}\int_0^1G(x,\xi)\frac{1}{\xi}\left(\frac{d\bar{w}^*_d}{d\xi}\right)^2d\xi \tag{71b}$$

Using the Krylov-Bogoliubov-Mitropolsky (KBM) perturbation method [45] and solving the nonlinear dynamic Eq. (68), one can obtain the amplitude-frequency relations as

$$\alpha=\frac{\omega}{\omega_n}=1+\frac{1}{24}\left(9\mu_2-10\mu_1^2\right)\hat{a}^2+\frac{5}{8}\mu_1\mu_2\hat{a}^3+\ldots \tag{72}$$

Note that the ratio is unity, $\alpha=\omega/\omega_n=1$ if the system is linear. Normalizing the test function

$$\bar{w}^*_d(0)=\operatorname*{Max}_{x\in[0,1]}\left[\bar{w}^*_d(x)\right]=1 \tag{73}$$

One finds that $\hat{a}$ represents the normalized dimensionless vibration amplitude at the center of the piezoelectric laminated circular FGM plate. Furthermore, using Eq. (49), one can write the dimensionless amplitude at the center of the plate as

$$\hat{a}=\bar{w}_d\big|_{r=0}=2\sqrt{3\left(1-\nu^2\right)}\left.\frac{w_d}{h_f}\right|_{r=0} \tag{74}$$

Table 5. FGM index effects to the first normalized mode shape.

Radial Distance (r/a)	FGM index (n) / Normalized Voltage (V)									
	Metal			n=100			n=10			
	V=0	V=2	V=3.8	V=0	V=2	V=3.8	V=0	V=2	V=3.8	
0.0	*0.9991*	*0.9972*	*0.9964*	*0.9989*	*0.9970*	*0.9962*	*0.9987*	*0.9968*	*0.9960*	
0.2	*0.9589*	*0.9509*	*0.9401*	*0.9576*	*0.9496*	*0.9388*	*0.9562*	*0.9483*	*0.9375*	
0.4	*0.8105*	*0.7882*	*0.7659*	*0.8081*	*0.7858*	*0.7635*	*0.8056*	*0.7833*	*0.7610*	
0.6	*0.5758*	*0.5494*	*0.5184*	*0.5722*	*0.5458*	*0.5148*	*0.5687*	*0.5422*	*0.5113*	
0.8	*0.3018*	*0.2782*	*0.2518*	*0.2990*	*0.2754*	*0.2490*	*0.2962*	*0.2726*	*0.2462*	
1.0	*0.0029*	*0.0022*	*0.0020*	*0.0025*	*0.0018*	*0.0016*	*0.0021*	*0.0014*	*0.0012*	
	n=1			n=0.1			Ceramic (n=0)			
	V=0	V=2	V=3.8	V=0	V=2	V=3.8	V=0	V=2	V=3.8	
0.0	*0.9985*	*0.9966*	*0.9958*	*0.9983*	*0.9964*	*0.9956*	*0.9981*	*0.9962*	*0.9954*	
0.2	*0.9549*	*0.9470*	*0.9362*	*0.9536*	*0.9457*	*0.9349*	*0.9523*	*0.9443*	*0.9335*	
0.4	*0.8032*	*0.7809*	*0.7586*	*0.8008*	*0.7785*	*0.7562*	*0.7983*	*0.7760*	*0.7537*	
0.6	*0.5651*	*0.5387*	*0.5077*	*0.5615*	*0.5351*	*0.5041*	*0.5580*	*0.5316*	*0.5006*	
0.8	*0.2934*	*0.2698*	*0.2434*	*0.2906*	*0.2670*	*0.2406*	*0.2878*	*0.2642*	*0.2378*	
1.0	*0.0017*	*0.0010*	*0.0008*	*0.0013*	*0.0006*	*0.0004*	*0.0009*	*0.0002*	*0.0000*	

Table 6. FGM index and normalized voltage effects to the second normalized mode shape.

Radial Distance (r/a)	FGM index (n) / Normalized Voltage (V)											
	Metal		n=100		n=10		n=1		Ceramic (n=0)	
	V=0	V=3	V=0	V=3	V=0	V=3	V=0	V=3	V=0	V=3
0.0	*1.0000*	*1.0000*	*1.0000*	*1.0000*	*0.9999*	*0.9999*	*0.9999*	*0.9999*	*0.9998*	*0.9998*
0.1	*0.9415*	*0.9300*	*0.9413*	*0.9298*	*0.9411*	*0.9296*	*0.9409*	*0.9294*	*0.9405*	*0.9290*
0.2	*0.7416*	*0.7343*	*0.7413*	*0.7340*	*0.7409*	*0.7336*	*0.7406*	*0.7333*	*0.7399*	*0.7327*
0.3	*0.4540*	*0.4441*	*0.4535*	*0.4437*	*0.4531*	*0.4432*	*0.4526*	*0.4427*	*0.4517*	*0.4418*
0.4	*0.1437*	*0.1228*	*0.1431*	*0.1222*	*0.1425*	*0.1216*	*0.1419*	*0.1210*	*0.1407*	*0.1197*
0.5	*-0.1285*	*-0.1608*	*-0.1292*	*-0.1615*	*-0.1300*	*-0.1623*	*-0.1307*	*-0.1630*	*-0.1322*	*-0.1645*
0.6	*-0.3150*	*-0.3507*	*-0.3159*	*-0.3516*	*-0.3168*	*-0.3525*	*-0.3176*	*-0.3533*	*-0.3194*	*-0.3551*
0.7	*-0.3879*	*-0.4161*	*-0.3890*	*-0.4171*	*-0.3900*	*-0.4181*	*-0.3910*	*-0.4192*	*-0.3931*	*-0.4212*
0.8	*-0.3426*	*-0.3566*	*-0.3433*	*-0.3573*	*-0.3440*	*-0.3580*	*-0.3447*	*-0.3587*	*-0.3461*	*-0.3601*
0.9	*-0.1985*	*-0.2008*	*-0.1989*	*-0.2012*	*-0.1993*	*-0.2016*	*-0.1997*	*-0.2020*	*-0.2005*	*-0.2028*
1	*0.0000*	*0.0000*	*-0.0001*	*-0.0001*	*-0.0002*	*-0.0002*	*-0.0003*	*-0.0003*	*-0.0005*	*-0.0005*

Table 7. Normalized voltage effects to the frequency dependent amplitude changes of the first two modes for metal plate.

Central Deflection	First Mode (ω/ω_1)				Second Mode (ω/ω_2)			
	V=0	V=1	V=1.5	V=2	V=0	V=1	V=1.5	V=2
0.0	*1.0000*	*1.0000*	*1.0000*	*1.0000*	*1.0000*	*1.0000*	*1.0000*	*1.0000*
0.1	*1.0029*	*0.9962*	*0.9964*	*0.9955*	*1.0031*	*1.0023*	*1.0026*	*1.0007*
0.2	*1.0203*	*0.9967*	*0.9949*	*0.9946*	*1.0098*	*1.0094*	*1.0090*	*1.0040*
0.3	*1.0486*	*0.9966*	*0.9912*	*0.9899*	*1.0214*	*1.0198*	*1.0189*	*1.0084*
0.4	*1.0866*	*0.9984*	*0.9871*	*0.9828*	*1.0385*	*1.0345*	*1.0333*	*1.0138*
0.5	*1.1337*	*1.0060*	*0.9856*	*0.9773*	*1.0610*	*1.0540*	*1.0524*	*1.0207*
0.6	*1.1900*	*1.0229*	*0.9894*	*0.9765*	*1.0881*	*1.0785*	*1.0758*	*1.0291*
0.7	*1.2560*	*1.0504*	*0.9995*	*0.9810*	*1.1195*	*1.1072*	*1.1026*	*1.0392*
0.8	*1.3334*	*1.0896*	*1.0167*	*0.9892*	*1.1555*	*1.1392*	*1.1323*	*1.0516*
0.9	*1.4259*	*1.1446*	*1.0435*	*1.0002*	*1.1966*	*1.1745*	*1.1654*	*1.0654*
1	*1.5405*	*1.2280*	*1.0880*	*1.0190*	*1.2440*	*1.2160*	*1.2050*	*1.0799*

Recall that all the quantities presented in this section are dimensionless, and are normalized with respect to known parameters.

6. Case studies, results and discussions

In this section, the nonlinear static deformation, and the linear and nonlinear vibrations in the vicinity of the nonlinearly deformed static positions of a simply supported piezoelectric bounded FGM circular plate are studied. The control effects (both static and dynamic effects) induced by the normalized control voltages are investigated. From the methods discussed in the preceding sections, a computer program was developed and numerical solutions were acquired and analyzed. Since the nonlinear dynamic analysis is built upon the nonlinear static analysis, static results are presented first, followed by the dynamic solutions.

Before going further into the results and discussion, since there were no published results for the compound piezoelectric FGM plate we decided to verify the validity of obtained results with those of FEM results. Our FEM model for piezo-FG plate comprises a 3D 8-noded solid element with 3 DOF per node (translation) in the host plate element and 6 DOF per node (3 translation, temperature, voltage and magnetic properties) in the piezoelectric element. Table 2 compares the present results of normalized dimensionless central deflections $W_s = \sqrt{3\left(1-\nu^2\right)}\left(w_s/h_f\right)$ with finite element solutions in analyzing the effect of normalized dimensionless piezoelectric voltages $V = \left[3(1-\nu^2)\right]^{1/2} e_{31}(h_f + h_p)V^* \Big/ \left(2D_2 h_f\right)$ to the normalized dimensionless center deflections in which a nonlinear deflection-voltage relationship can be observed. As it is seen from Table 2 the maximum difference between the proposed solutions and finite element method is about 0.073 % and a close correlation between these results validates the proposed method of solution.

As shown in Fig. 2 the effect of imposed voltage to the center deflection is nonlinear and this effect is predominant in lesser voltage amounts.

Having validated the foregoing formulations, we begin to study the large amplitude vibration behavior of FG laminated circular plates that are subjected to electro-mechanical preloading. The results for laminated plates with isotropic substrate layers (that is, the substrate is purely metallic or purely ceramic) and with graded substrate layers (various n) are given in both tabular and graphical forms.

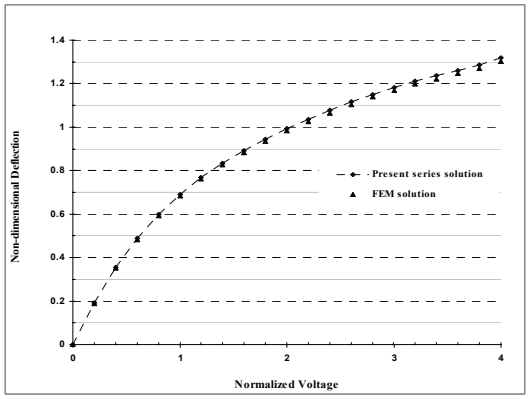

Fig. 2. Comparison between the proposed series solution and FEM in analyzing the effect of normalized piezoelectric voltages to the dimensionless center deflections.

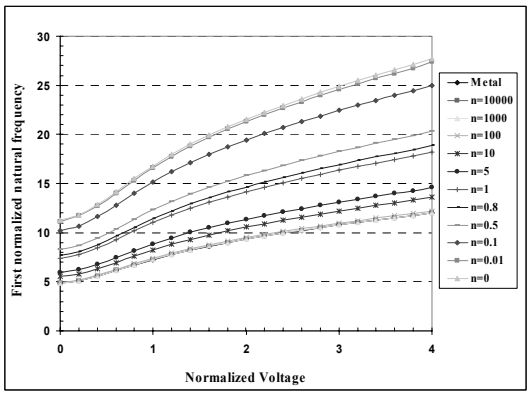

Fig. 3. Effect of control voltages to the first normalized natural frequency for various FGM indexes.

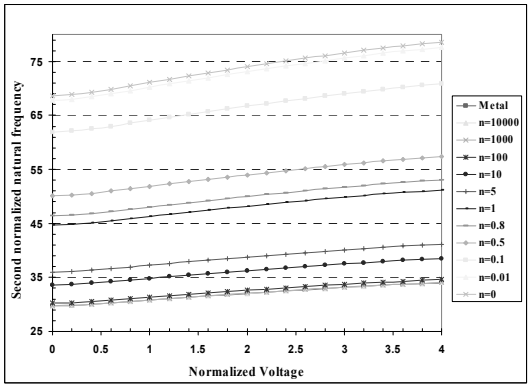

Fig. 4. Changes of the second natural frequency versus control voltages.

We examine in this section the effect of control voltages to the vibration characteristics of the piezoelectric laminated circular FG plate for various FGM

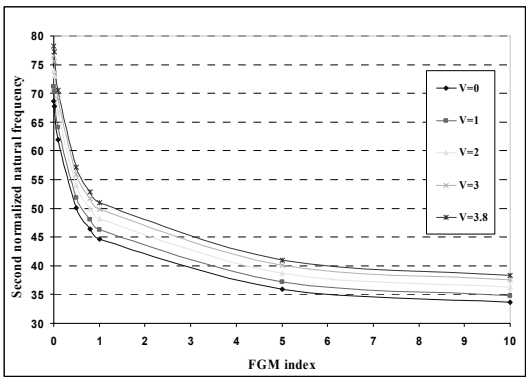

Fig. 5. Effect of FGM index to the second natural frequency.

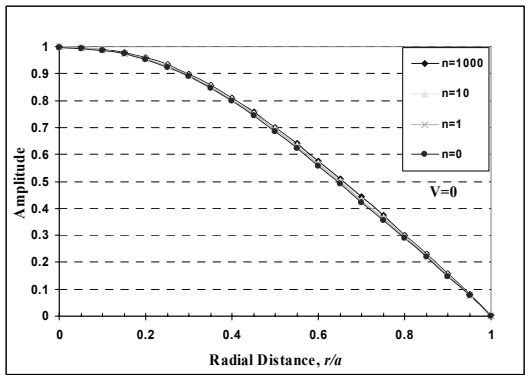

Fig. 6. FGM index effects to the first normalized mode shape for V=0.

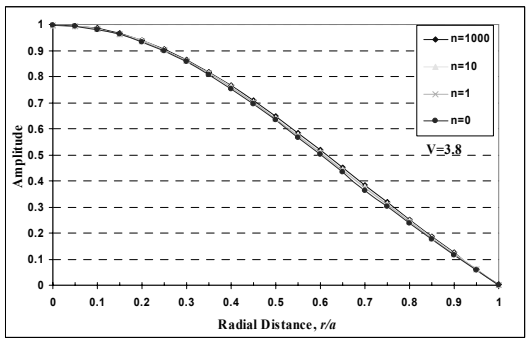

Fig. 7. FGM index effects to the first normalized mode shape for V=3.8.

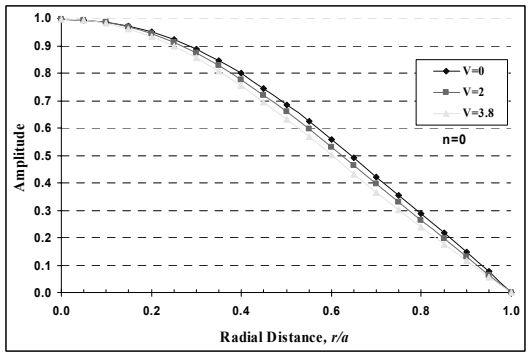

Fig. 8. Voltage effects to the first normalized mode shape (n=0).

indexes. To this end, Tables 3, 4 as well as Figs. 3, 4, 5 show the nonlinear relationships between first two natural frequencies $\omega_i a^2\sqrt{I_1/D_2}$, versus the dimensionless control voltages V . These free vibrations are assumed to be in the vicinity of the nonlinearly deformed static equilibrium position.

Table 3 and Fig. 3 show the effect of normalized control voltage to the first natural frequency of the FG circular plate for various FGM indexes. It is seen that, for FGM plate with n=10 by increasing the imposed voltage from 1 to 2 (100%) first natural frequency increases about 28.4% while by increasing the voltage from 2 to 4 (100%) first natural frequency increases about 28.6%.

Table 4 and Fig. 4 show the effect of normalized control voltages to the second natural frequency of the FGM circular plate for various FGM indexes. As it shows, for FGM plate with n=10 by increasing the imposed voltage from 1 to 2 (100%) the first natural frequency increases about 4.06% while by increasing the voltage from 2 to 4 (100%) the first natural frequency increases 6.24%.

Also from Table 3 and Table 4, the effect of applied control voltage is more dominant to the first natural frequency compared to its effect to the second natural frequency; e.g., while n=10, by increasing the normalized imposed voltage from 0 to 4 the first natural frequency increases about 145.5% while the second natural frequency increases about 14.5%. It is worthy of note that the influence of the applied voltage is much more significant on the lower-order frequencies, especially on the fundamental frequencies, and it tends to be much weaker on higher-order vibration frequencies. Since the lower-order frequencies are generally of the greatest importance in determining the dynamic response of a plate, this feature indicates the great possibility of suppressing the dynamic deflections of pre-stressed FG circular plates by using the piezoelectric materials.

Also, Fig. 5 illustrates the effect of FGM index on the normalized second frequency of the structure. The mode shapes of first two natural modes are also studied as the control voltage changes. The results are

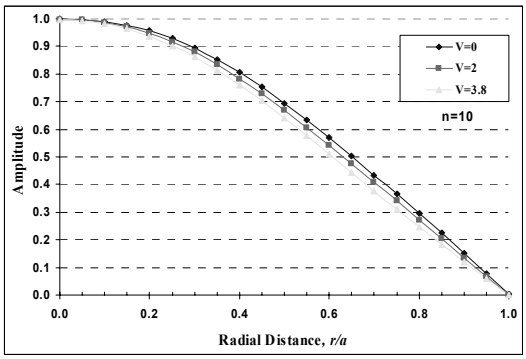

Fig. 9. Voltage effects to the first normalized mode shape (n=10).

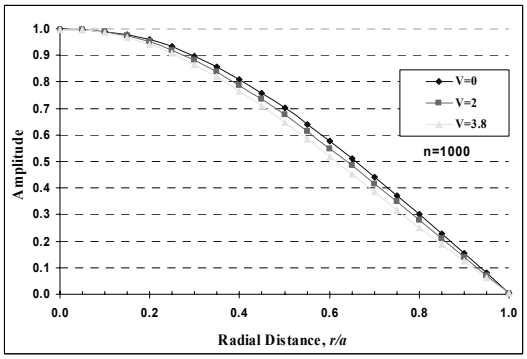

Fig. 10. Voltage effects to the first normalized mode shape (n=1000).

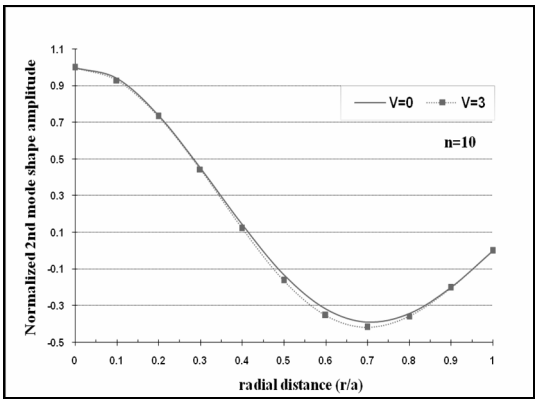

Fig. 11. Normalized voltage effects to the second normalized mode shape for n=10.

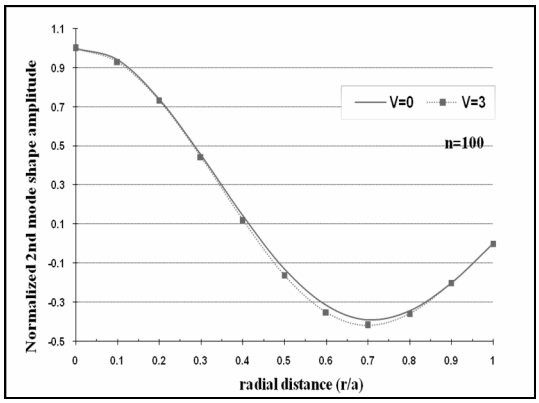

Fig. 12. Normalized voltage effects to the second normalized mode shape for n=100.

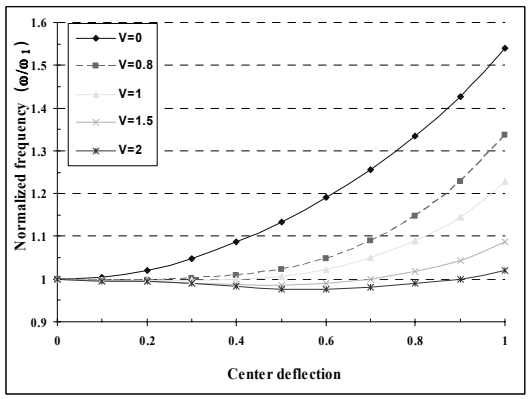

Fig. 13. First natural frequency (ω/ω_1) and amplitude (w/h_f) relations for different control voltages (V=0, 0.8, 1, 1.5, 2).

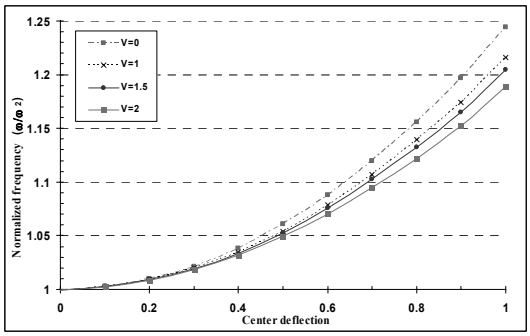

Fig. 14. Second natural frequency (ω/ω_2) and amplitude (w/h_f) relations for different control voltages (V=0, 1, 1.5, 2).

tabulated in Table 5 and the effect of FGM indexes is illustrated for (*V=0, 3.8*) in Figs. 6, 7 and the voltage effect is shown for (*n=0, 10,100*) in Figs. 8, 9, 10.

Table 6 shows the effect of control voltages on the second normalized mode shape amplitude of the FG circular plate for various FGM indexes and for various radial distances (r/a). As it shows, for FGM plate with n=10 by imposing the voltage for the amount of V=3 the second normalized mode shape decreases by 7.21% for (r/a=0.7) while it decreases by 2.18% for (r/a=0.3). For better viewing these effects, Figs. 11

and 12 are illustrated showing the effect of applied control voltages on the second normalized mode shape of the FG circular plate for various radial distances (r/a) and with two FGM indexes (n=10) and (n=100) respectively.

Also the effect of normalized voltage on the frequency dependent amplitude changes of the first two modes are investigated and tabulated in Table 7 while the frequency dependent amplitude changes of the first two modes are plotted in Figs. 13 and 14. In each figure, the effects of control voltages are also included. Note that all quantities presented in this section are normalized dimensionless quantities.

7. Summary and conclusions

The static, dynamic and control effects of a piezoelectric bounded FGM circular plate with an initial nonlinear large static deformation (the von-Karman type geometrical nonlinear deformation) have been studied. System electromechanical equations incorporating the nonlinear deformation were derived first. An exact solution technique based on series-type solutions was used to solve for analytical solutions of nonlinear static and eigenvalue problems of the nonlinearly deformed circular plate. Large amplitude effects were studied by the Galerkin method and the perturbation method. Numeric results suggested that both the static and dynamic behavior of the nonlinear circular FG plate with various FGM indexes can be controlled by the control voltages applied to the piezoelectric actuator layers. The analytical and numerical results suggest that first, the natural frequencies of small amplitude vibrations in the vicinity of the nonlinearly deformed static equilibrium position increase as the piezoelectric voltage increases for all values of FGM indexes. The control effect on the first mode is more prominent than on the second mode for all values of FGM indexes, because the piezoelectric actuator layers are fully distributed on the plate. Since the lower-order frequencies are generally of the greatest importance in determining the dynamic response of a plate, this feature indicates the great possibility of suppressing the dynamic deflections of pre-stressed FG circular plates by using the piezoelectric materials. Second, the control effects on natural mode shapes are minimal. Basically, these mode shapes remain about the same as their original mode shapes. Third, studies of nonlinear frequency-amplitude relations suggest that control voltages can bring the nonlinearities back to their linear regions. Thus, with proper control voltages, undesired nonlinear oscillations in FG plates can be controlled to manageable linear oscillations, even further to actively damped oscillations. Accordingly, overall system performance can be significantly improved.

Acknowledgments

This research was funded by the research deputy of the University of Tehran (Project No. 8106002/6/02).

References

[1] M. Teymur, N. R. Chitkara, K. Yohngjo, J. Aboudi, M. J. Pindera and S. M. Arnold, Thermoelastic Theory for the Response of Materials Functionally Graded in Two Directions, *Int. J. Solids Struct.*, 33 (1996) 931-966.

[2] M. Koizumi, The concept of FGM, *Ceram. Trans. Funct. Grad. Mater*. 34 (1993) 3-10.

[3] T. Bailey and J. E. Hubbard, Distributed piezoelectric polymer active vibration control of a cantilever beam, *J. Guid. Control Dyn.*, 8 (1985) 605-611.

[4] S. E. Miller and J. E. Hubbard, Observability of a Bernoulli–Euler beam using PVF2 as a distributed sensor, *MIT Draper Laboratory Report, (*1987).

[5] S. Dong and L. Tong, Vibration control of plates using discretely distributed piezoelectric quasi-modal actuators/sensors, AIAA *J.,* 39 (2001) 1766-1772.

[6] M. C. Ray, Optimal control of laminated shells with piezoelectric sensor and actuator layers, *AIAA J.*, 41 (2003) 1151-1157.

[7] F. Peng, A. Ng and Y. R. Hu, Actuator placement optimization and adaptive vibration control of plate smart structures, *J. Intell. Mater. Syst. Struct*., 16 (2005) 263-271.

[8] W. J. Spencer, W. T. Corbett, L. R. Dominguez and B. D. Shafer, An electronically controlled piezoelectric insulin pump and valves, *IEEE Trans. Sonics Ultrason.*, 25 (1978) 153-156.

[9] S. Dong, X. Du, P. Bouchilloux and K. Uchino, Piezoelectric ring-morph actuation for valve application, *J. Electroceram*., 8 (2002) 155-161.

[10] C. Y. K. Chee, L. Tong and G. P. Steve, A review on the modeling of piezoelectric sensors and actuators incorporated in intelligent structures, *J. Intell. Mater. Syst. Struct.,* 9 (1998) 3-19.

[11] L. Cao, S. Mantell and D. Polla, Design and simu-

lation of an implantable medical drug delivery system using microelectromechanical systems technology, *Sensors Actuators A*, 94 (2001) 117-125.

[12] X. Chen, C. H. J. Fox and S. Mc William, Optimization of a cantilever microswitch with piezoelectric actuation, *J. Intell. Mater. Syst. Struct.,* 15 (2004) 823-834.

[13] A. B. Dobrucki and P. Pruchnicki, Theory of piezoelectric axisymmetric bimorph Sensors, Actuators A 58 (1997) 203-212.

[14] C. J. Morris and F. K. Forster, Optimization of a circular piezoelectric bimorph for a micropump driver, *J. Micromech.Microeng*. 10 (2000) 459-465.

[15] S. Li and S. Chen, Analytical analysis of a circular PZT actuator for valveless micropump, *Sensors Actuators A*, 104 (2003) 151-161.

[16] E. F. Crawley and E. H. Anderson, Detailed models of piezoceramic actuation of beams, *J. Intell. Mater. Syst. Struct.,* 1 (1990) 4-25.

[17] S. Timoshenko, Theory of Plates and Shells, Second Ed. McGraw-Hill, New York, (1940).

[18] H. S. Tzou, Piezoelectric Shells-Distributed Sensing and Control of Continua, Kluwer Dordrecht, (1993).

[19] H. S. Tzou and J. P. Zhong, Electromechanics and vibrations of piezoelectric shell distributed systems theory and applications ASME, J of Dynamic Systems, *Measurements, and Control*, 115 (3) (1993) 506-517.

[20] Y. Ootao and Y. Tanigawa, Control of transient thermoelastic displacement of a functionally graded rectangular plate bonded to a piezoelectric plate due to nonuniform heating, *Acta Mech.,* 148 (2001) 17-33.

[21] J. N. Reddy and Z. Q. Cheng, Three-dimensional solutions of smart functionally graded plates, *ASME J. Appl. Mech.,* 68 (2001) 234-241.

[22] B. L. Wang and N. Noda, Design of smart functionally graded thermo-piezoelectric composite structure, *Smart Mater. Struct.,* 10 (2001) 189-193.

[23] X. Q. He, T. Y. Ng, S. Sivashanker and K. M. Liew, Active control of FGM plates with integrated piezoelectric sensors and actuators, *Int. J. Solids Struct.,* 38 (2001) 1641-1655.

[24] K. M. Liew, J. Yang and S. Kitipornchai, Post buckling of piezoelectric FGM plates subject to thermo-electro-mechanical loading, *Int. J. Solids Struct.,* 40 (2003) 3869-3892.

[25] H. S. Shen, Post buckling of FGM plates with piezoelectric actuators under thermo-electro-mechanical loadings, *Int. J. Solids Struct.,* 42 (2005) 6101-6612.

[26] J. Yang, S. Kitipornchai and K. M. Liew, Nonlinear analysis of thermo-electro-mechanical behavior of shear deformable FGM plates with piezoelectric actuators, *Int. J. Numer. Methods Eng.,* 59 (2004) 1605-1632.

[27] J. Yang, S. Kitipornchai and K. M. Liew, Large amplitude vibration of thermo-electric-mechanically stressed FGM laminated plates, Comput. *Methods Appl. Mech. Eng.,* 192 (2003) 3861-3885.

[28] X. L. Huang and H. S. Shen, Vibration and dynamic response of functionally graded plates with piezoelectric actuators in thermal environments, *J. Sound Vib.,* 289 (2006) 25-53.

[29] F. Ebrahimi, A. Rastgoo and M. H. Kargarnovin, Analytical investigation on axisymmetric free vibrations of moderately thick circular functionally graded plate integrated with piezoelectric layers, *Journal of Mechanical Science and Technology*, 22 (6) (2008) 1056-1072.

[30] F. Ebrahimi and A. Rastgoo, Free vibration analysis of smart annular FGM plates integrated with piezoelectric layers, *Smart Mater. Struct.,* 17 (2008) No. 015044.

[31] F. Ebrahimi and A. Rastgoo, An analytical study on the free vibration of smart circular thin FGM plate based on classical plate theory, *Thin-Walled Structures*, 46 (2008) 1402-1408.

[32] F. Ebrahimi, A. Rastgoo and A. A. Atai, theoretical analysis of smart moderately thick shear deformable annular functionally graded plate, *European Journal of Mechanics - A/Solids*, published online: 25 Dec. 2008.

[33] F. Ebrahimi and A. Rastgoo, Free Vibration Analysis of Smart FGM Plates, *International Journal of Mechanical Systems Science and Engineering*, 2 (2) (2008) 94-99.

[34] J. N. Reddy and G. N. Praveen, Nonlinear transient thermoelastic analysis of functionally graded ceramic-metal plate, *Int. J. Solids Struct.*, 35 (1998) 4457-4476.

[35] X. L. Huang and H. S. Shen, Nonlinear vibration and dynamic response of functionally graded plates in thermal environment. *International Journal of Solids and Structures*, 41 (2004) 2403–2427.

[36] R. C. Wetherhold, S. Seelman and S.Wang, The use of functionally graded materials to eliminate or control thermal deformation, *Compos. Sci. Technol.,* 56 (1996) 1099-1104.

[37] Y. Tanigawa, H. Morishita and S. Ogaki, Derivation of system of fundamental equations for a three dimensional thermoelastic field with nonhomogeneous material properties and its application to a semi infinite body, *J. Therm. Stresses*, 22 (1999) 689-711.

[38] D. O. Brush and B. O. Almroth, *Buckling of Bars Plates and Shells*, McGraw-Hill, New York, (1975).

[39] J. N. Reddy, *Theory and Analysis of Elastic Plates*, Taylor and Francis, Philadelphia, (1999).

[40] G. Song, V. Sethi and H. N. Lic, Vibration control of civil structures using piezoceramic smart materials: A review, *Engineering Structures*, 28 (2006) 1513-1524.

[41] E. Efraim and M. Eisenberger, Exact vibration analysis of variable thickness thick annular isotropic and FGM plate, *J. Sound Vib.,* 299 (2007) 720-738.

[42] C. Y. Chia, *Nonlinear Analysis of Plates*, McGraw-Hill, New York, (1980).

[43] X. J. Zheng and Y. H. Zhou, Analytical formulas of solutions of geometrically nonlinear equations of axisymmetric plates and shallow shells, *Acta Mech. Sinica*, 6 (1) (1990) 69-81.

[44] H. P. William, P. F. Brain and A. T. Sau, Numerical Recipes-the Art of Scientific Computing, Cambridge University Press, New York, (1986).

[45] A. H. Nayfe and D. T. Mook, *Nonlinear Oscillations*, John Wiley, New York, (1979).

Farzad Ebrahimi received his B.S. and M.S. degree in Mechanical Engineering from University of Tehran, Iran. He is currently working on his Ph.D. thesis under the title of "Vibration analysis of smart functionally graded plates" at Smart Materials and Structures Lab in Faculty of Mechanical Engineering of the University of Tehran. His research interests include vibration analysis of plates and shells, smart materials and structures and functionally graded materials.